ACS APPLIED MATERIALS & INTERFACES

Research Article

www.acsami.org

Free Standing Reduced Graphene Oxide Film Cathodes for Lithium Ion Batteries

Sung Hoon Ha, Yo Sub Jeong, and Yun Jung Lee*

Department of Energy Engineering, Hanyang University, Seoul 133-791, Republic of Korea

Supporting Information

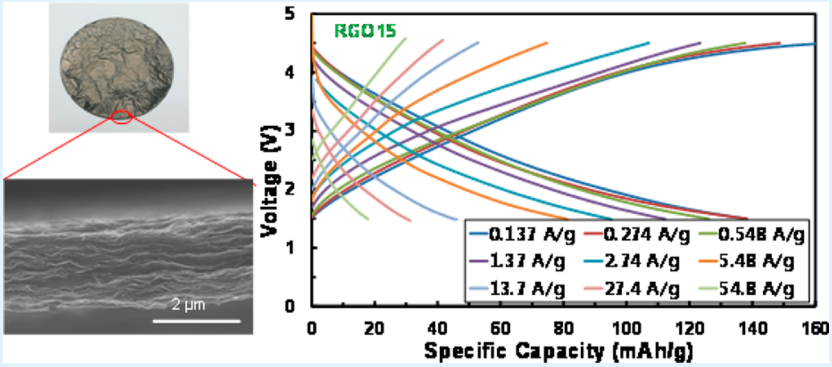

ABSTRACT: We report the fabrication and electrochemical activity of free-standing reduced graphene oxide (RGO) films as cathode materials for lithium ion batteries. The conducting additive and binder-free RGO electrodes with different oxygen contents were assembled by a simple vacuum filtration process from aqueous RGO colloids prepared with the aid of cationic surfactants. The gravimetric capacity of RGO film cathodes showed clear dependence on the oxygen contents controlled by the thermal reduction process. The capacity increased with the increase of the amount of oxygen functional groups, indicating that the main lithium capturing mechanism of RGO cathodes is Li^+ ion interaction with the surface oxygen functionalities. The hydroxyl groups (C−OH) as well as carbon−oxygen double bonds have been identified as the lithiation-active species. The RGO cathodes achieved excellent rate capability due to the fast surface Faradaic reaction, suggesting that self-supported RGO films are promising cathodes for high power application. The graphene oxide (GO)/RGO composite films showed inferior performance to those of RGO only. The poor electronic conductivity of GO might result in inefficient utilization of redox active oxygen functional groups despite the higher oxygen content and higher theoretical capacity of GO/RGO composite films. Further optimization on the amount of oxygen functional groups for higher capacity and better electronic conductivity would lead to the development of RGO based high energy-high power cathodes.

KEYWORDS: *graphene, lithium ion battery, cathodes, free-standing films, high power*

1. INTRODUCTION

As an intriguing nanomaterial, an ideal graphene is one-atom thick two-dimensional (2D) hexagonal lattice of tightly packed monolayer of carbon atoms.[1] Interest in this material has surged over the past few years because of its unique physical and chemical properties and potential applications to various fields including gas sensors,[2,3] hydrogen storage,[4,5] electronic devices such as transistors,[6] field emission displays,[7,8] and so on. Especially, its outstanding electrical and thermal conductivity, superior mechanical flexibility, a broad electrochemical window, along with the high specific surface area have made graphene a promising electrode material for various electrochemical energy devices such as supercapacitors,[9−12] batteries,[13−16] fuel cells,[17−20] and solar cells.[21−23] Of special interest is the electrochemical interaction of lithium with graphene in lithium ion batteries (LIBs). Graphene based electrodes were reported to accommodate lithium more readily than the common graphite anode due to additional reaction mechanisms other than intercalation, such as fast lithium adsorption,[24−26] defect trapping,[27] and double layer or faradaic capacitance.[28] However, most studies on graphene as electrode materials in LIB systems focused on applying graphene as an advanced carbonaceous material to replace the graphite anode, to which lithium ions intercalate at a low voltage window below 1.5 V vs Li/Li^+.[13−16,29−34] Utilization of advanced carbonaceous materials as cathodes for lithium ion batteries has been limited so far. Recently, functionalized carbon nanotubes (CNTs) have been reported to interact with lithium ions in the voltage window above 1.5 V vs Li/Li^+, where it can be stated as cathodes.[35−37] The origin of interaction between lithium ions and CNT in this potential range has been ascribed to the presence of oxygen functional groups on the surface of carbon.

Received: June 5, 2013
Accepted: November 14, 2013
Published: November 14, 2013

The reaction between lithium ions and carbonyl/carboxylic acid functional groups are known to occur at ~3 V vs Li/Li^+.[35,38] The fast pseudocapacitive surface reaction (Faradaic redox reaction) enabled enhanced high power performances since the kinetic limitation imposed by the extremely slow solid state diffusion could be avoided.

Motivated by these recent findings, we set out to systematically explore the interaction between lithium ions and the graphene with surface oxygen functional groups as cathodes for LIBs. Herein, we fabricated free-standing reduce graphene oxide (RGO) films and evaluated electrochemical activity as cathodes for LIBs. The RGO is a functionalized graphene, reduced from graphene oxide (GO) with various surface oxygen functionalities. The amount of oxygen functionalities can be adjusted by controlling the reduction process.[9,39] Here, RGOs with C/O ratios of 15, 25, and 110 were prepared by controlling thermal annealing temperature. Free standing films without additional conducting additives and binders were used as electrodes. The need for conducting additives and binders in the conventional electrode fabrication processes could be eluded by using self-supporting graphene films with high electrical conductivity and excellent mechanical flexibility/stability.[15,40] The binder-free electrode configuration could further improve a high rate capability by allowing better accessibility for the electrolytes and increasing electronic conductivity.[34] Free standing paper-like electrodes are also useful in the development of flexible and wearable energy storage devices.[16] The free-standing RGO film cathodes showed a systematic increase in capacity with the oxygen contents of RGO, confirming the role of oxygen functionalities in faradaic redox reaction between lithium ions and functionalized carbon. RGO cathodes demonstrated excellent rate capability due to the fast surface redox reaction, suggesting that free-standing RGO films are promising cathodes for high power application of LIBs. The composite between RGO and GO showed inferior performances to those of RGO only films. While pristine GO or GO/RGO composites have higher oxygen contents and higher theoretical capacities, RGO only films with tunable oxygen contents are more promising in terms of efficient utilization of redox active sites to obtain higher capacity (high energy) as well as better kinetics (high power). Although other parameters such as porous microstructures or surface areas might also affect the energy-power performances,[41,42] further optimization on the amount of oxygen functional groups between higher capacity (high C/O ratio) and better electronic conductivity (low C/O ratio) for better kinetics would lead to the development of RGO based high energy-high power cathodes.

2. EXPERIMENTAL SECTION

2.1. Material Synthesis. GO was prepared by a modified Hummers method.[43] To oxidize graphite to graphite oxide first, 3.33 g of natural graphite (Alfa Aesar, powder, <325 mesh) was added to 100 mL of H_2SO_4 (98%) at room temperature. The mixture was placed in an ice bath followed by a slow addition of 10.5 g of $KMnO_4$. The resulting solution was stirred for 90 min. The mixture then was moved to an oil bath at 50 °C and stirred for 1 h. Subsequent addition of 150 mL of water caused a rapid rise in temperature to ~95 °C, and the mixture was stirred for 1 h. Finally, 11.67 mL of H_2O_2 (30 wt %) was added to the mixture. After cooling to room temperature, the solution was filtered and washed with aqueous HCl (10 wt %, 1 L) and copious amount of water until the solution pH reached ~5.0. Then, the synthesized graphite oxide was exfoliated and dispersed in water by ultrasonication. The resulting aqueous GO solution was centrifuged in order to eliminate remaining graphite oxide aggregates.

RGO was produced by thermal reduction from GO. Dried GO powder was charged into a quartz tube and annealed under Ar/4% H_2 atmosphere at various temperatures for 3 h. The ramping rate was 30 °C min^{-1}. The RGO powder thus prepared was dispersed in water with the aid of surfactants. In a typical preparation of RGO dispersion, 200 mg of RGO (with different oxygen contents) was added to a 200 mL aqueous solution of cetyltrimetylammonium bromide (CTAB) and stirred for 30 min. The solution was sonicated for 1 h in tip horn sonicator (BRANSON SONIFER 450D, 450 W, 55% amplitude). The resultant solution was centrifuged for 15 min at 10 000 rpm, and the upper 80% of the supernatant was carefully taken out. The concentration of RGO colloids was determined by measuring the mass of RGO film made by vacuum filtration through the Anodisc membrane filter (AAO, 47 mm or 25 mm, 0.2 μm pore size, Whatman). For free-standing RGO film formation, appropriate amount of aqueous RGO colloid was vacuum-filtered on AAO to have mass loading of ~1 mg cm^{-2}. After thorough washing with ethanol and water, the RGO film on AAO was completely dried under room temperature and then detached from the AAO support. The detached RGO film was further dried in an oven at 80 °C overnight.

2.2. Characterization. The morphologies and thickness of RGO films were examined by scanning electron microscopy (SEM, Nova NanoSEM 450). Thermogravimetric analysis (TGA, TG-DTA 2000SA) was carried out on the RGO films to determine the residual surfactant content of the sample. Reduction of GO to RGO was monitored by chemical analysis by X-ray photoelectron spectroscopy (XPS, theta probe base system).

2.3. Electrochemical Test. The free-standing RGO films were tested as cathodes without additional carbon or binder. The RGO film dried overnight in an oven at 80 °C was cut into the desired size and used as it is without further processing. The coin cells were assembled in an argon-filled glovebox using a lithium metal as the counter electrode and Celgard 2600 as the separator. The electrolyte was 1 M $LiPF_6$ solution in a 1:1 mixture of ethylene carbonate (EC) and dimethyl carbonate (DMC). The galvanostatic tests were performed using the battery tester (Maccor series 4000) at room temperature with a potential range from 1.5 to 4.5 V. For the XPS surface analysis, the cells employing RGO15 cathodes were disassembled in a glovebox after the first discharge or the first recharge and the tested RGO film cathode was recovered, washed three times with DMC solution and dried.

3. RESULTS AND DISCUSSION

RGOs with different oxygen contents were prepared by thermal reduction of GO in Ar/4% H_2 at various temperatures. The atomic ratio C/O was quantified by XPS analysis from the area ratio of C1s and O1s peaks. Figure 1a shows the representative XPS survey scans of pristine GO, RGO annealed at 650, 750, and 1000 °C. The intensity of O1s peaks was progressively reduced with increasing reduction temperature, while that of C1s peaks was enhanced, indicating thermal reduction at elevated temperatures. The C/O atomic ratios of RGO reduced at various temperature in Ar/4% H_2 are summarized in Figure 1b. C/O ratio of pristine GO before thermal treatment was 2.49, and C/O of thermally treated RGO decreased significantly to 15 after the heat reduction at 650 °C, 25 at 750 °C, and 110 at 1000 °C in Ar/4% H_2.

Free standing RGO films were assembled by vacuum filtration of the RGO dispersion in water (Figure 2). The RGO powder with different oxygen contents was first dispersed in an aqueous cationic surfactant CTAB solution. The concentration of aqueous RGO colloids showed clear dependence on the C/O ratio of RGO; as C/O ratio increased, concentration of RGO colloids decreased. Colloidal concentrations of RGOs in water were 0.08, 0.04, and 0.03 mg mL^{-1}

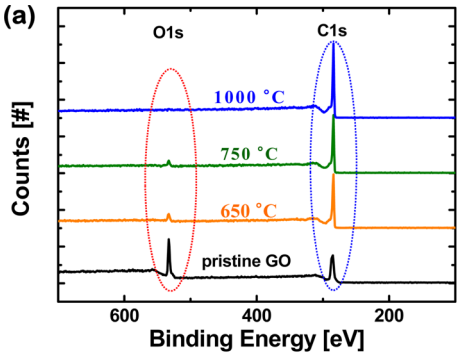

(b)

	C/O Atomic Ratio	Oxygen percent (%)
Pristine GO	2.5	29
600 °C	12	7.7
650 °C	15	6.3
700 °C	19	5.0
750 °C	25	3.8
800 °C	43	2.3
1000 °C	110	0.9

Figure 1. XPS chemical analysis of RGOs reduced at different temperature under Ar/4% H_2 atmosphere. (a) Survey scans of pristine GO, RGO annealed at 650, 750, and 1000 °C. (b) Summary of atomic ratios C/O from the intensities of C1s and O1s peaks at various temperatures.

for C/O ratios of 15, 25, and 110, respectively. We expect higher hydrophobicity for RGO surfaces with increasing C/O ratios leading to higher interfacial energy with water. Therefore, the graphene sheets with higher C/O ratio experience higher van der Waals attractions enhancing flocculation tendency of the RGO dispersion. Aggregated RGO sheets were removed from the solution by centrifuge resulting lower colloidal concentrations with increasing C/O ratio. The aqueous RGO colloids were vacuum filtered through the AAO membrane filter, and the formed RGO films were peeled off to create free-standing, paperlike RGO electrodes. The resulting RGO film with a mass loading of ~1 mg cm^{-2} had a typical thickness of ~2.5 μm. SEM images of RGO films showed the typical wrinkled lamellar structures of stacked 2D sheets. The RGO films made from RGO with C/O = 15, 25, and 110 were named RGO15, RGO25, and RGO110, respectively, and selected for further test as LIB cathodes.

Surfactant mass contents, carefully determined by TGA, were excluded from the mass of RGO films to correctly determine the mass of RGO electrodes. The representative TGA curves of RGO powder with C/O = 15, CTAB surfactant, and RGO15 dispersed with CTAB are given in Figure S1 (Supporting Information). After through washing with water and ethanol, RGO15 films made from RGO15 dispersed with CTAB had only ~1 wt % residual CTAB. In addition, CTAB was previously reported inactive with lithium.[44] Therefore, we could exclude the contribution of CTAB to the capacity.

The electrochemical performances of the rGO cathodes with different oxygen contents in lithium ion batteries were galvanostatically evaluated in the voltage range 1.5–4.5 V vs Li/Li^+. Figure 3 shows the specific capacities of RGO15, RGO25, and RGO110 cathodes at 0.137 A g^{-1} for 30 cycles. Typical galvanostatic charge–discharge curves are shown in Figure 3a with the RGO15 cathode. The potential profile changes gradually without any plateau in both charge and discharge. The charge–discharge curves in Figure 3a were very stable after the first few cycles. The initial discharge capacity of the RGO 15 cathode was ~125 mAh g^{-1} and stabilized to 110–115 mAh g^{-1} within the first five cycles in Figure 3b. The role of surface oxygen functionalities on the gravimetric capacities is clearly demonstrated in Figure 3b–d. The initial discharge capacity of RGO25 cathode was 80 mAh g^{-1} and the capacities were rapidly stabilized to 75 mAh g^{-1}. With the highest C/O and lowest oxygen content RGO110 electrode, the stable reversible capacity was ~20 mAh g^{-1}. The Coulombic

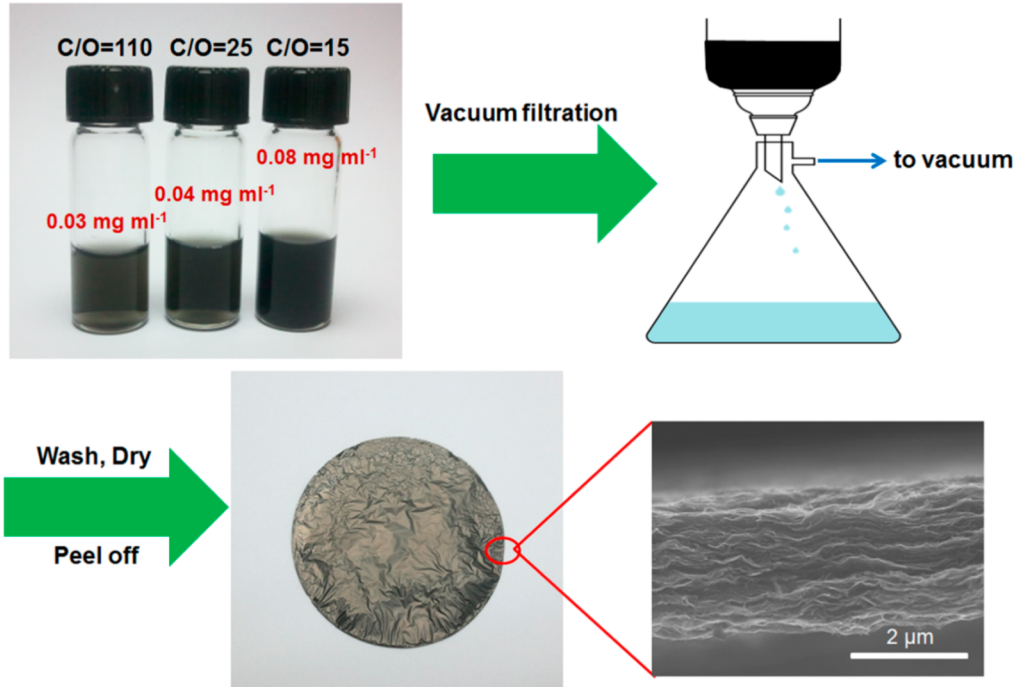

Figure 2. Fabrication process of free-standing RGO films and cross-sectional SEM image of the RGO film.

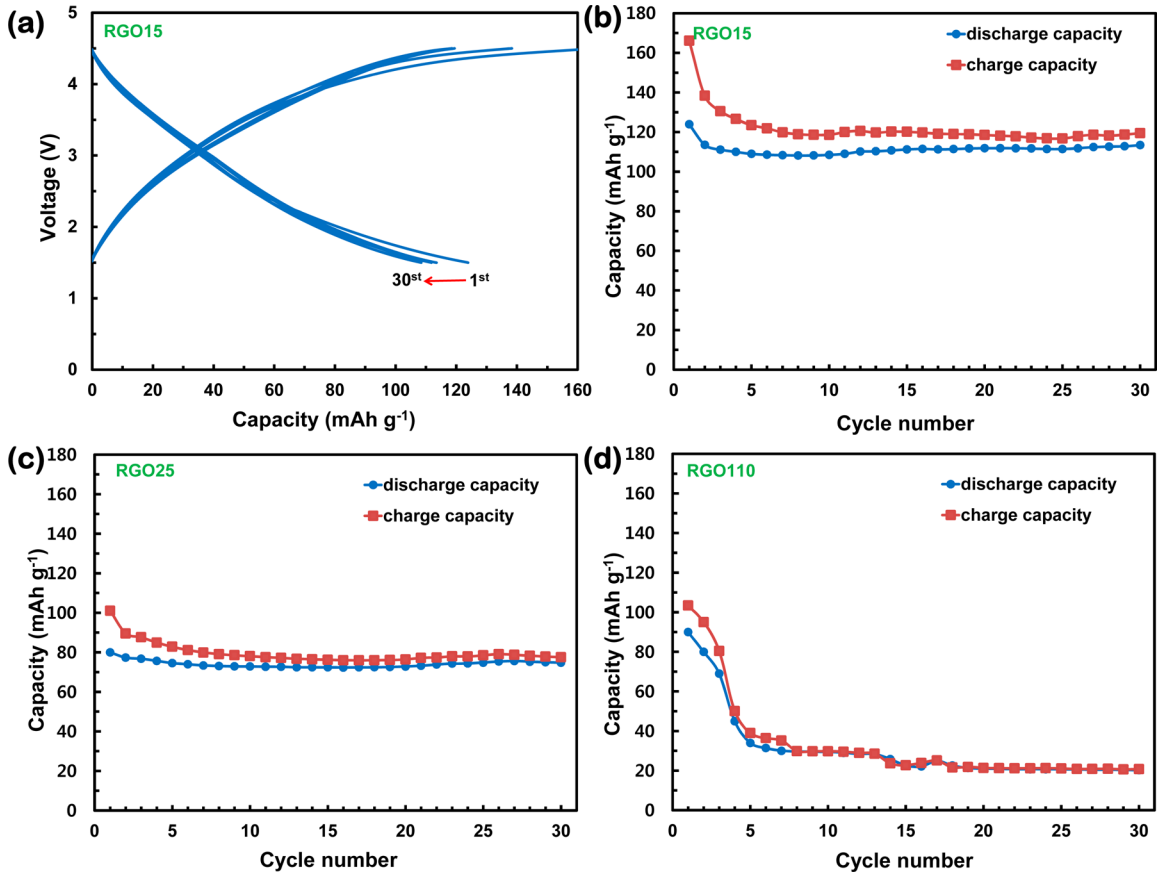

Figure 3. Cathode performances of RGO15, RGO25, and RGO110 films at 0.137 A g^{-1} for 30 cycles. (a) Charge−discharge curves of RGO15, (b) cyclability of RGO15, (c) cyclability of RGO25, and (d) cyclability of RGO110.

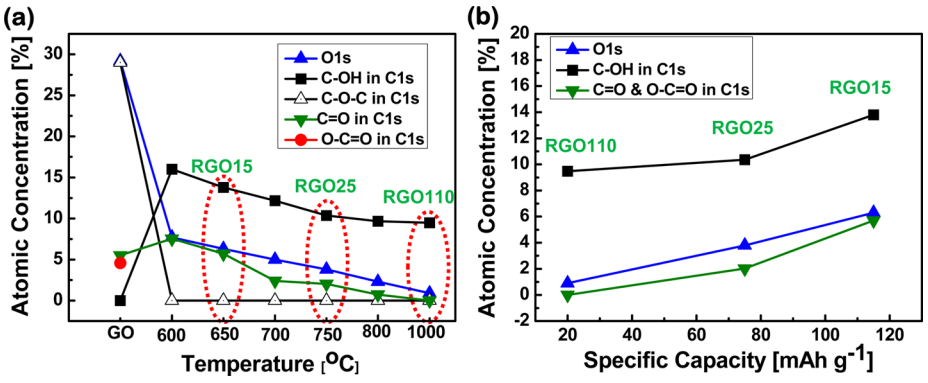

Figure 4. (a) Atomic concentration of O1s and oxygen functional groups in C1s in GO and RGOs prepared at different temperatures. (b) Relationship between discharge capacity and the atomic concentration of O1s and oxygen functional groups in C1s. The discharge capacities are the stabilized values tested at 0.137 A g^{-1} for 30 cycles in Figure 3 and the oxygen functional groups in C1s are hydroxyl (C−OH) and carbonyl or carboxyl (C═O or O−C═O) since epoxide is absent in RGO15, 25, and 100 films.

efficiencies (CEs) in Figure 3b−d are presented in Figure S2. The CEs of the first cycles were 75−80%; however, they rapidly increased >95% for the RGO film cathodes under study. Despite the possible contribution from the double layer capacitance to the total capacity, the relationship between the total oxygen content and the apparent capacity provides clear inference that the redox reactions of lithium ions and the surface oxygen functional groups are the primary lithium capturing mechanism in the functionalized carbon cathodes. If we consider the faradaic reaction of surface oxygen, for example, the carbonyl group (C═O) with lithium in the voltage range >1.5 V vs Li/Li^+ such as $C{=}O_{graphene} + Li^+ + e^- \leftrightarrow C{-}OLi_{graphene}$,[35] the theoretical specific capacities can be calculated as 137, 85, and 20 mAh g^{-1} for RGO15, RGO25, and RGO110, respectively. Although there is a controversy on the main lithium storage species among the surface oxygen functional groups of functionalized carbon whether it is carbon−oxygen double bond[35,45] or epoxide,[46] this calculation would be valid as long as each oxygen reacts with one lithium ion and all oxygen functionalities are fully reactive. We tentatively assumed that all surface oxygen functionalities present on the RGO films under study could electrochemically

dx.doi.org/10.1021/am4044147 | ACS Appl. Mater. Interfaces 2013, 5, 12295−12303

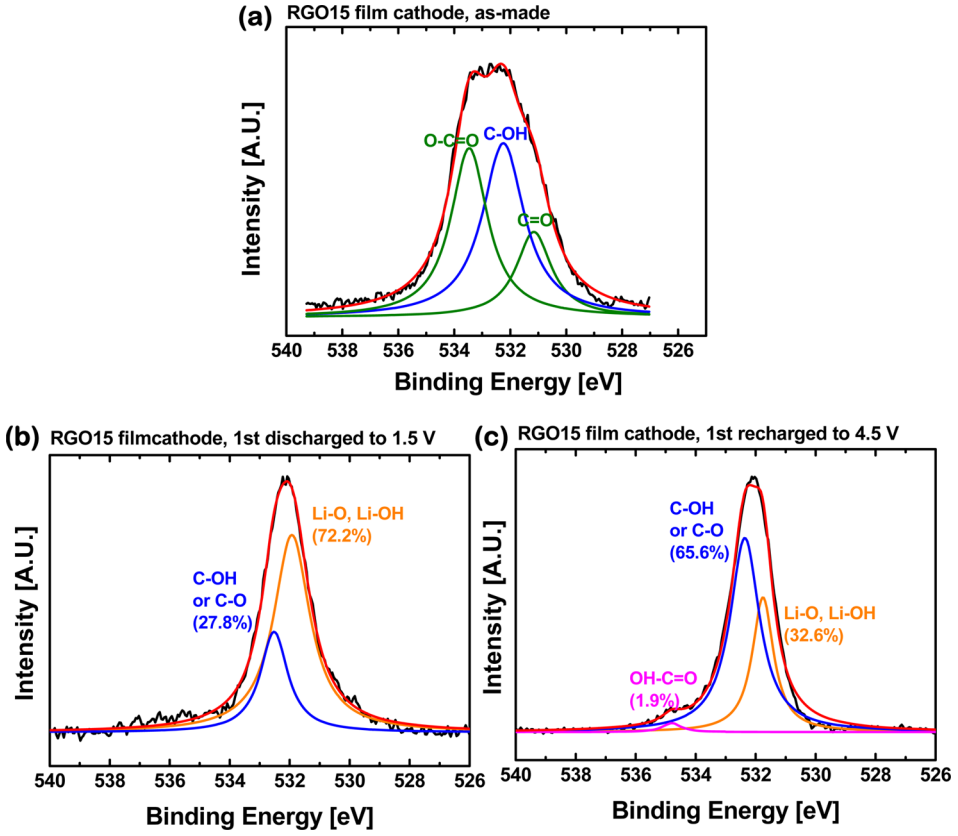

Figure 5. Ex situ XPS O1s spectra of the (a) as-made, (b) discharged, and (c) recharged RGO15 film cathodes.

react with lithium ions and store one lithium ion per oxygen for theoretical capacity calculation.

To identify oxygen functional groups on the RGO films under study and the contribution of different functional groups to the lithium storage, surface chemical attributes were analyzed by XPS survey and high resolution C1s. High resolution C1s spectra of RGOs annealed at 650, 750, and 1000 °C are presented in Figure S3. Figure 4a is the atomic concentration of total oxygen O1s and different functional groups in C1s in the as-made GO and RGOs thermally treated at different temperatures. GO has 29% C−O−C (epoxide), 5.5% C═O (carbonyl), and 4.6% O−C═O (carboxyl) with 29% total oxygen. As shown in Figure 1b, total oxygen content showed systematic decrease from GO (29%) to RGO annealed at 1000 °C (0.9%). The C−O−C epoxides were not detected in the annealed samples. Instead, the amount of C−OH (hydroxyl) groups was first increased to 16% upon annealing at 600 °C similar to the previous report[46] and then decreased with annealing temperature. It is difficult to clearly separate C═O and O−C═O peaks in the RGOs annealed at ≥600 °C. The amount of combined C═O and O−C═O also decreased with the annealing temperature. Overall, the amount of total oxygen and all the oxygen functional groups present in the annealed RGOs decreased as the thermal treatment temperature increased. To further determine the role of each oxygen functional group in lithium storage, the discharge capacities of the RGO15, RGO25, and RGO110 cathodes were plotted versus the atomic concentration of O 1s and oxygen functional groups that constitute the C 1s peaks (Figure 4b). As indicated, it is clear that the capacity decreased as the total oxygen concentration decreased. The specific capacity scales with the amount of hydroxyl as well as that of the carbon−oxygen double bond (C═O and O−C═O) suggesting that both hydroxyl and carbon−oxygen double bond are reactive with lithium ions.

To confirm the proposed redox centers for lithium storage, variations of oxygen groups upon discharge and recharge have been traced by ex situ XPS O1s spectra for the as-made, first discharged and first recharged RGO15 cathodes in Figure 5. Consistent with the high resolution C1s spectrum in Figure S3a, O1s spectrum of as-made RGO15 cathode contains C−OH, O−C═O, and C═O. Upon reacting with lithium (discharge), the intensity of O−C═O and C−OH peaks reduced and the peak related to Li−O/Li−OH substantially increased. Subsequent lithium removal during recharge decreased Li−O/Li−OH peak intensity and increased C−OH/C−O peak along with the slight evolution of OH-C═O. This result indicates that lithium ions are first stored both in C−OH (hydroxyl) and the carbon−oxygen double bonds such as C═O (carbonyl) and O−C═O (carboxyl) in our system. While C−OH bonds were reversibly delithiated during recharge, O−C═O groups were only slightly restored, suggesting that carboxylic bonds were converted to other species such as C−OH/C−O during redox reaction with lithium. Previously, carbon−oxygen double bonds (carbonyl and carboxyl)[35,45] and epoxide[46] have been reported as the active species with lithium ions. In the present study, hydroxyl groups were also found to reversibly react with lithium ions. It could be concluded that most surface oxygen functional groups reported for the functionalized carbon surface (epoxide, hydroxyl, carbonyl, and carboxyl) could store lithium ions; however, depending on the surface composition, the main redox center in act appeared differently in the individual study.

The utilization percentage of the active redox species (measured specific capacity/theoretical capacity) in each electrode was 84% for RGO15 (compared to theoretical capacity of 137 mAh g^{-1}), while that of RGO25 and RGO110 was 88% and 100%, respectively. Although the absolute specific capacities of the RGOs with higher C/O ratio were smaller than those of RGOs with lower C/O, the utilization efficiency of the redox active species appeared higher probably due to the higher electronic conductivity of the RGOs with lower oxygen contents. One should note that the initial capacity of highly reduced RGO110 was ~90 mAh g^{-1}, much higher than the theoretical capacity based on the redox reaction of oxygen-containing groups, and it decayed fast. The origin of this irreversible capacity is not totally clear at this moment; however, we speculate that this irreversible capacity might be related to the defects such as vacancies and five or seven membered rings present on the RGO surface, where the undesirable side reactions could be catalyzed.

While the high energy density is also of interest, the high power performances comparable to and even exceeding that of the supercapacitor, is the main motivation for exploring functionalized carbon cathodes in LIB system. Rate capability of the free-standing RGO15 cathode was tested in the current range from 0.137 to 54.8 A g^{-1} in Figure 6. The specific capacities decreased with increasing rates (currents), but more than half of the theoretical capacity (80 mAh g^{-1}) was delivered at current of 5.48 A g^{-1}. This indicates that capacity of 80 mAh g^{-1} can be charged in 53 s. The fast surface Faradaic reaction of oxygen functional groups enabled excellent rate capability demonstrated here, suggesting that self-supported RGO films are promising cathodes for high power application of LIBs. Ragone plot in Figure 6b clearly shows the excellent high-power performance of the free-standing RGO film cathode. The high power performance of RGO15 cathode was slightly better than the best result reported for CNT + graphene freestanding electrode[37] probably due to a higher C/O ratio of the RGO15 film.

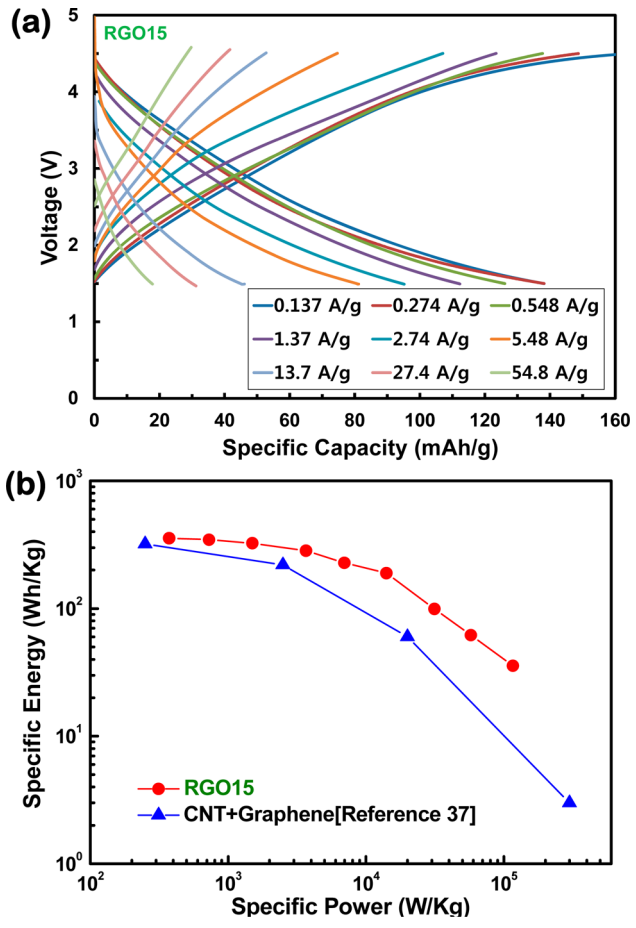

Figure 6. Rate capability of RGO15 film cathodes. (a) Charge–discharge curves at different rates and (b) Ragone plot. The result for CNT + graphene is shown for comparison.

Considering the role of surface oxygen functionalities as active redox species in LIB cathodes, we tried to include pristine GO in the cathode structure to increase gravimetric capacities. The theoretical capacity of GO with C/O=2.49 is 584 mAh g^{-1} based on the faradaic reaction of the carbonyl (C═O) or carboxylic (O−C═O) group with lithium. Since pristine GO is electrically insulating, composites between RGO 15 and GO were fabricated to electrically wire the insulating GO. The performance of pristine GO in GO and conducting carbon composite cathodes have been reported previously.[46] Figure 7 shows the schematic of producing GO/RGO15 composite by a self-assembling process. Appropriate amounts of aqueous RGO15 solution dispersed with CTAB and GO solutions were mixed together. The electrostatic attraction between the negatively charged GO surface and the positive charges on CTAB attached to RGO15 leads to the self-assembled, stacked lamellar structures of GO-RGO15. The interaction of positively charged RGO15 dispersed with CTAB and negatively charged GO was manifested by the formation of visible aggregates upon mixing of the two solutions. The resulting solution was briefly sonicated to deflocculate for the preparation of uniform film by vacuum filtration. After the GO/RGO15 composite film formation, CTABs between GO and RGO15 sheets were removed by excessive washing with ethanol and water.

The mass ratio of GO/rGO = 5:5 and 8:2 composites were tested as cathodes in LIB cells. Figure 8 shows the specific capacities of these composites at 0.137 A g^{-1} for 30 cycles. The theoretical capacity of the composites were 361 and 495 mAh g^{-1} for 5:5 and 8:2 composites, respectively, based on the theoretical capacity of RGO15 (137 mAh g^{-1}) and GO (584 mAh g^{-1}). In Figure 8a and b, the 5:5 composite delivered initial discharge capacity of 150 mAh g^{-1}, but capacities were stabilized to 55 mAh g^{-1}. Similarly, the 8:2 composite showed initial discharge capacity of 365 mAh g^{-1} and dropped rapidly to the 80 mAh g^{-1}. Although the capacities were stable after 10th cycle, irreversibility in the first few cycle is severe for GO/RGO15 composites. The utilization percentage of active sites (measured specific capacity/theoretical capacity) was only about 15% for both composites. Overall, the cathode performances of GO/RGO15 composite films were inferior to those of RGO15 only film. A previous report on the GO/functionalized MWNT hierarchical composite[37] also showed slightly better properties than our GO/RGO composites. We speculate that the inferior performances were ascribed to the different stacking mechanism of 2D GO/RGO sheets from that of GO/MWNT hierarchical composites. In preparing GO/functionalized MWNT hierarchical composite, both GO and MWNT assume negative surface charges and there is no mutual attractive interaction between the two nanocarbons involved. The random stacking between GO and MWNT would have a higher possibility of forming a percolating conducting network

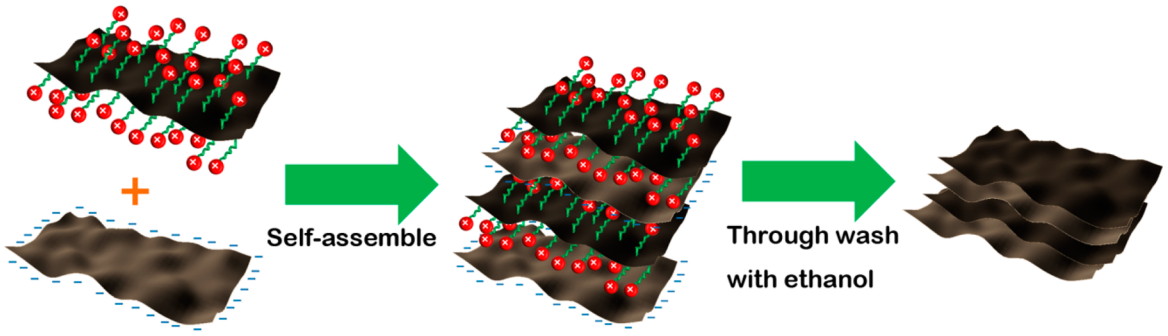

Figure 7. Schematic of GO/RGO15 composite formation process.

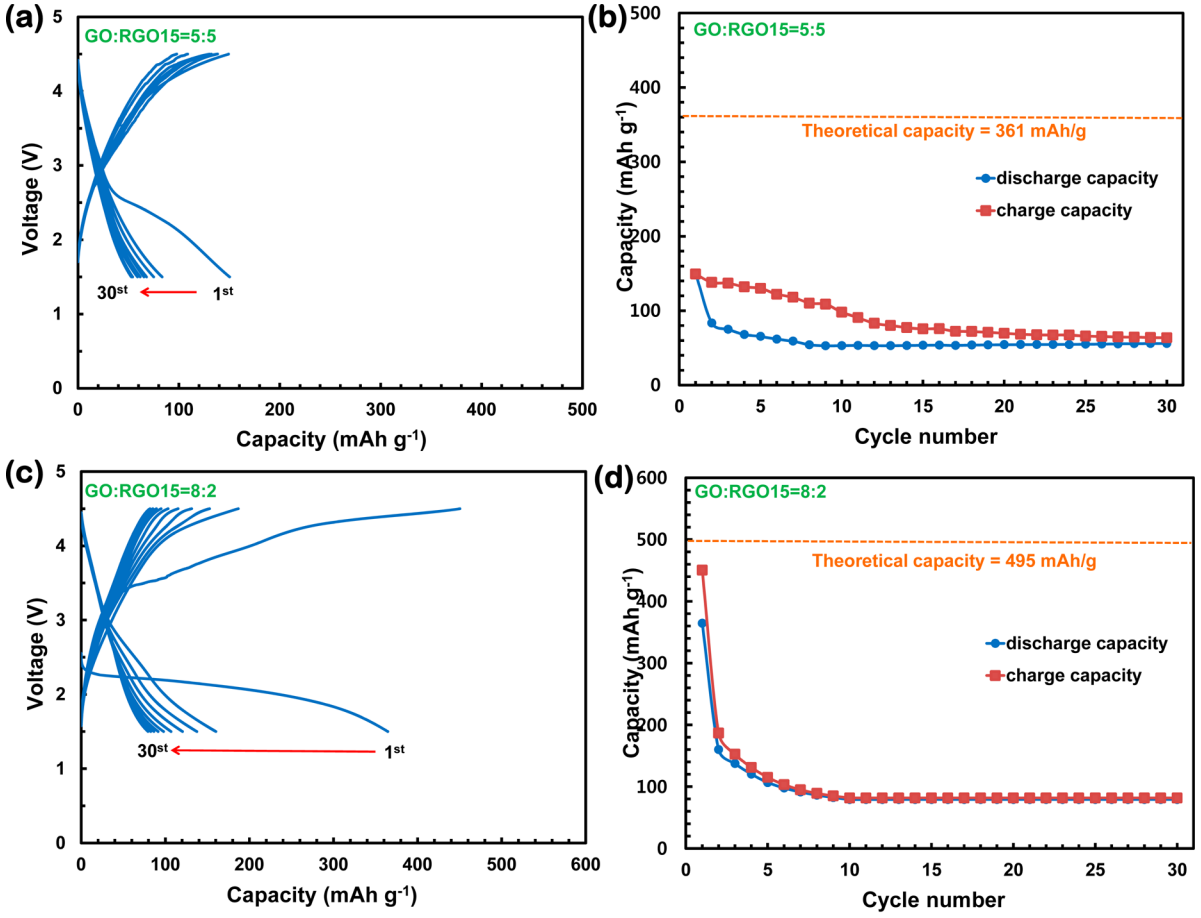

Figure 8. Cathode performances of GO/RGO15 composite films at 0.137 A g^{-1} for 30 cycles. (a) Charge−discharge curves of GO/RGO15 = 5:5 films, (b) cyclability of GO/RGO15 = 5:5 films, (c) charge−discharge curves of GO/RGO15 = 8:2 films, and (d) cyclability GO/RGO15 = 8:2 films.

of MWNTs to electrically wire insulating GO between MWNTs. On the other hand, the electrostatic interaction between positive charges on CTAB anchored on RGO and negative charges on GO surface would lead to sequential stacking of RGO and GO as shown in Figure 7. The resulting lamellar structure of sequential RGO and GO could electrically isolate RGO by insulating GO which could lead to inefficient electrical wiring, resulting inferior performances. Even for GO/functionalized MWNT hierarchical composite, the utilization percentage of active sites was only 35%.[37] This indicates that while pristine GO or GO/RGO composites have higher oxygen contents and higher theoretical capacities, poor electronic conductivity of GO prevent efficient utilization of active redox sites. In this regard, RGO only films with tunable oxygen contents are more promising to obtain higher capacity (high energy) as well as better kinetics (high power). Although other parameters such as porous microstructures or surface areas might also affect the energy-power performances,[41,42] further optimization on the amount of oxygen functional groups between higher capacity (high C/O ratio) and better electronic conductivity (low C/O ratio) would lead to the development of RGO based high energy-high power cathodes.

4. CONCLUSIONS

Free standing RGO films were assembled by a simple vacuum filtration method from aqueous RGO colloids prepared in a

dx.doi.org/10.1021/am4044147 | ACS Appl. Mater. Interfaces 2013, 5, 12295−12303

cationic surfactant solution. RGOs with different amount of surface oxygen functionalized were produced by controlling the thermal reduction process. RGOs with C/O ratios of 15, 25, and 110 were prepared. When conductive additive and binder-free RGO films were tested as cathodes in LIB cells, the gravimetric capacity demonstrated a systematic decrease with the increase of C/O ratio (decrease of the amount of surface oxygen functional groups), confirming the role of oxygen functionalities in Faradaic redox reaction between lithium ions and functionalized carbon. The oxygen functional groups in RGO films under study were C−OH and carbon−oxygen double bonds (C═O (carbonyl) and/or O−C═O (carboxyl)) and all these functional groups interacted with lithium ions. The RGO cathodes achieved excellent rate capability due to the fast surface Faradaic reaction, suggesting that self-supported RGO films are promising cathodes for high power application. The RGO15 electrodes showed a specific discharge capacity of 125 mAh g^{-1} at the first cycle at 0.137 A g^{-1} rate, which corresponds to ∼91% of the theoretical capacity of C/O=15 cathodes (137 mAh g^{-1}) and delivered ∼115 mAh g^{-1} at 1.37 A g^{-1} and 82 mAh g^{-1} at 5.48 A g^{-1}. The composite between RGO and GO showed inferior performances to those of RGO only films. The utilization percentage of active sites was only ∼15%. The lamellar structure formed by sequential restacking between RGO and GO could electrically isolate RGO by insulating GO. The films thus formed could display inefficient electrical wiring of active redox materials, resulting inferior performances. While pristine GO or GO/RGO composites have higher oxygen content and higher theoretical capacities, RGO only films with tunable oxygen contents are more promising in terms of efficient utilization of redox active sites to obtain higher capacity (high energy) as well as better kinetics (high power). To realize the RGO based high energy-high power cathodes, optimization on the oxygen functional groups for the best performances is needed between higher capacity (high C/O ratio) and better electronic conductivity (low C/O ratio) for better kinetics.

■ ASSOCIATED CONTENT

Supporting Information

TGA curves of RGO 15 only, CTAB only and CTAB-RGO15 (Figure S1), Coulombic efficiencies of RGO cathodes in Figure 3b −d (Figure S2), and high resolution C1s XPS spectra of RGOs thermally treated at 650, 750, and 1000 °C (Figure S3). This material is available free of charge via the Internet at http://pubs.acs.org.

■ AUTHOR INFORMATION

Corresponding Author

*E-mail: yjlee94@hanyang.ac.kr.

Notes

The authors declare no competing financial interest.

■ ACKNOWLEDGMENTS

This work was supported by Basic Science Research Program through the National Research Foundation of Korea (NRF) funded by the Ministry of Education, Science and Technology (Grant Nos. 2012R1A1A1009029 and 2012R1A1A2021678).

■ REFERENCES

(1) Geim, A. K.; Novoselov, K. S. *Nat. Mater.* **2007**, *6*, 183−191.
(2) Fowler, J. D.; Allen, M. J.; Tung, V. C.; Yang, Y.; Kaner, R. B.; Weiller, B. H. *ACS Nano* **2009**, *3*, 301−306.
(3) Li, W.; Geng, X.; Guo, Y.; Rong, J.; Gong, Y.; Wu, L.; Zhang, X.; Li, P.; Xu, J.; Cheng, G.; Sun, M.; Liu, L. *ACS Nano* **2011**, *5*, 6955−6961.
(4) Wang, L.; Lee, K.; Sun, Y.-Y.; Lucking, M.; Chen, Z.; Zhao, J. J.; Zhang, S. B. *ACS Nano* **2009**, *3*, 2995−3000.
(5) Wang, Y.; Guo, C. X.; Wang, X.; Guan, C.; Yang, H.; Wang, K.; Li, C. M. *Energy Environ. Sci.* **2011**, *4*, 195−200.
(6) Zheng, J. X.; Wang, L.; Quhe, R. G.; Liu, Q. H.; Li, H.; Yu, D. P.; Mei, W. N.; Shi, J. J.; Gao, Z. X.; Lu, J. *Sci. Rep.* **2013**, *3*, 1314.
(7) Wu, Z.-S.; Pei, S.; Ren, W.; Tang, D.; Gao, L.; Liu, B.; Li, F.; Liu, C.; Cheng, H.-M. *Adv. Mater.* **2009**, *21*, 1756−1760.
(8) Yu, S.-S.; Zheng, W.-T. *Nanoscale* **2010**, *2*, 1069−1082.
(9) Wu, X. Z.; Zhou, J.; Xing, W.; Wang, G. Q.; Cui, H. Y.; Zhuo, S. P.; Xue, Q. Z.; Yan, Z. F.; Qiao, S. Z. *J. Mater. Chem.* **2012**, *22*, 23186−23193.
(10) Wang, D.-W.; Li, F.; Zhao, J.; Ren, W.; Chen, Z.-G.; Tan, J.; Wu, Z.-S.; Gentle, I.; Lu, G. Q.; Cheng, H.-M. *ACS Nano* **2009**, *3*, 1745−1752.
(11) Wu, Z.-S.; Ren, W.; Wang, D.-W.; Li, F.; Liu, B.; Cheng, H.-M. *ACS Nano* **2010**, *4*, 5835−5842.
(12) Zhao, X.; Sanchez, B. M.; Dobson, P. J.; Grant, P. S. *Nanoscale* **2011**, *3*, 839−855.
(13) Yoo, E.; Kim, J.; Hosono, E.; Zhou, H.; Kudo, T.; Honma, I. *Nano Lett.* **2008**, *8*, 2277−2282.
(14) Bhardwaj, T.; Antic, A.; Pavan, B.; Barone, V.; Fahlman, B. D. *J. Am. Chem. Soc.* **2010**, *132*, 12556−12558.
(15) Zhao, X.; Hayner, C. M.; Kung, M. C.; Kung, H. H. *ACS Nano* **2011**, *5*, 8739−8749.
(16) Liu, F.; Song, S. Y.; Xue, D. F.; Zhang, H. J. *Adv. Mater.* **2012**, *24*, 1089−1094.
(17) He, D. P.; Cheng, K.; Peng, T.; Mu, S. C. *J. Mater. Chem. A* **2013**, *1*, 2126−2132.
(18) Seger, B.; Kamat, P. V. *J. Phys. Chem. C* **2009**, *113*, 7990−7995.
(19) Guo, S. J.; Dong, S. J.; Wang, E. K. *ACS Nano* **2010**, *4*, 547−555.
(20) Qu, L. T.; Liu, Y.; Baek, J. B.; Dai, L. M. *ACS Nano* **2010**, *4*, 1321−1326.
(21) Wang, X.; Zhi, L. J.; Mullen, K. *Nano Lett.* **2008**, *8*, 323−327.
(22) Bonaccorso, F.; Sun, Z.; Hasan, T.; Ferrari, A. C. *Nat. Photonics* **2010**, *4*, 611−622.
(23) Liu, Z. F.; Liu, Q.; Huang, Y.; Ma, Y. F.; Yin, S. G.; Zhang, X. Y.; Sun, W.; Chen, Y. S. *Adv. Mater.* **2008**, *20*, 3924−3930.
(24) Sato, K.; Noguchi, M.; Demachi, A.; Oki, N.; Endo, M. *Science* **1994**, *264*, 556−558.
(25) Dahn, J. R.; Zheng, T.; Liu, Y. H.; Xue, J. S. *Science* **1995**, *270*, 590−593.
(26) Xue, J. S.; Dahn, J. R. *J. Electrochem. Soc.* **1995**, *142*, 3668−3677.
(27) Pan, D. Y.; Wang, S.; Zhao, B.; Wu, M. H.; Zhang, H. J.; Wang, Y.; Jiao, Z. *Chem. Mater.* **2009**, *21*, 3136−3142.
(28) Yazami, R.; Deschamps, M. *J. Power Sources* **1995**, *54*, 411−415.
(29) Lian, P.; Zhu, X.; Liang, S.; Li, Z.; Yang, W.; Wang, H. *Electrochim. Acta* **2010**, *55*, 3909−3914.
(30) Reddy, A. L. M.; Srivastava, A.; Gowda, S. R.; Gullapalli, H.; Dubey, M.; Ajayan, P. M. *ACS Nano* **2010**, *4*, 6337−6342.
(31) Compton, O. C.; Jain, B.; Dikin, D. A.; Abouimrane, A.; Amine, K.; Nguyen, S. T. *ACS Nano* **2011**, *5*, 4380−4391.
(32) Wu, Z. S.; Ren, W. C.; Xu, L.; Li, F.; Cheng, H. M. *ACS Nano* **2011**, *5*, 5463−5471.
(33) Yang, Y. Q.; Pang, R. Q.; Zhou, X. J.; Zhang, Y. J.; Wu, H. X.; Guo, S. W. *J. Mater. Chem.* **2012**, *22*, 23194−23200.
(34) Wang, Z.-L.; Xu, D.; Wang, H.-G.; Wu, Z.; Zhang, X.-B. *ACS Nano* **2013**, *7*, 2422−2430.
(35) Lee, S. W.; Yabuuchi, N.; Gallant, B. M.; Chen, S.; Kim, B.-S.; Hammond, P. T.; Shao-Horn, Y. *Na. Nanotechnol.* **2010**, *5*, 531−537.
(36) Lee, S. W.; Gallant, B. M.; Lee, Y.; Yoshida, N.; Kim, D. Y.; Yamada, Y.; Noda, S.; Yamada, A.; Shao-Horn, Y. *Energy Environ. Sci.* **2012**, *5*, 5437−5444.

(37) Byon, H. R.; Gallant, B. M.; Lee, S. W.; Shao-Horn, Y. *Adv. Funct. Mater.* **2013**, *23*, 1037−1045.
(38) Chen, H.; Armand, M.; Demailly, G.; Dolhem, F.; Poizot, P.; Tarascon, J. M. *ChemSusChem* **2008**, *1*, 348−355.
(39) Ganguly, A.; Sharma, S.; Papakonstantinou, P.; Hamilton, J. *J. Phys. Chem. C* **2011**, *115*, 17009−17019.
(40) Gwon, H.; Kim, H. S.; Lee, K. U.; Seo, D. H.; Park, Y. C.; Lee, Y. S.; Ahn, B. T.; Kang, K. *Energy Environ. Sci.* **2011**, *4*, 1277−1283.
(41) Zhamu, A.; Chen, G. R.; Liu, C. G.; Neff, D.; Fang, Q.; Yu, Z. N.; Xiong, W.; Wang, Y. B.; Wang, X. Q.; Jang, B. Z. *Energy Environ. Sci.* **2012**, *5*, 5701−5707.
(42) Jang, B. Z.; Liu, C. G.; Neff, D.; Yu, Z. N.; Wang, M. C.; Xiong, W.; Zhamu, A. *Nano Lett.* **2011**, *11*, 3785−3791.
(43) Hummers, W. S.; Offeman, R. E. *J. Am. Chem. Soc.* **1958**, *80*, 1339−1339.
(44) Lee, Y. J.; Lee, Y.; Oh, D.; Chen, T.; Ceder, G.; Belcher, A. M. *Nano Lett.* **2010**, *10*, 2433−2440.
(45) Kim, H.; Lim, H. D.; Kim, S. W.; Hong, J.; Seo, D. H.; Kim, D. C.; Jeon, S.; Park, S.; Kang, K. *Sci. Rep.* **2013**, 3.
(46) Wang, D. W.; Sun, C. H.; Zhou, G. M.; Li, F.; Wen, L.; Donose, B. C.; Lu, G. Q.; Cheng, H. M.; Gentle, I. R. *J. Mater. Chem. A* **2013**, *1*, 3607−3612.